A Compact Atom Interferometer for Future Space Missions

Microgravity Sci. Technol.
DOI 10.1007/s12217-010-9240-7

ORIGINAL ARTICLE

A Compact Atom Interferometer for Future Space Missions

Fiodor Sorrentino · Kai Bongs · Philippe Bouyer · Luigi Cacciapuoti · Marella de Angelis · Hansjoerg Dittus · Wolfgang Ertmer · A. Giorgini · J. Hartwig · Matthias Hauth · Sven Herrmann · Massimo Inguscio · Endre Kajari · Thorben T. Könemann · Claus Lämmerzahl · Arnaud Landragin · Giovanni Modugno · Frank Pereira dos Santos · Achmin Peters · Marco Prevedelli · Ernst M. Rasel · Wolfgang P. Schleich · Malte Schmidt · Alexander Senger · Klaus Sengstock · Guillaume Stern · Guglielmo Maria Tino · Reinhold Walser

Received: 9 January 2010 / Accepted: 3 September 2010

Abstract Atom interferometry represents a quantum leap in the technology for the ultra-precise monitoring of accelerations and rotations and, therefore, for the science that relies on these quantities. These sensors evolved from a new kind of optics based on matter-waves rather than light-waves and might result in an advancement of the fundamental detection limits by several orders of magnitude. This paper describes the current status of the Space Atom Interferometer project (SAI), funded by the European Space Agency. In a multi-pronged approach, SAI aims to investigate both experimentally and theoretically the various

F. Sorrentino · M. de Angelis · A. Giorgini · G. M. Tino (✉)
Dipartimento di Fisica, Università di Firenze,
Polo Scientifico, via Sansone 1, 50019 Sesto Fiorentino, Italy
e-mail: guglielmo.tino@fi.infn.it

K. Bongs
Midlands Ultracold Atom Research Centre,
School of Physics & Astronomy, University of Birmingham,
Edgbaston, Birmingham B15 2TT, UK

P. Bouyer · G. Stern
Laboratoire Charles Fabry de L'Institut d'Optique,
Centre National de la Recherche Scientifique,
Campus Polytechnique Rd 128, 91127 Palaiseau, France

L. Cacciapuoti
Research and Scientific Support Department,
European Space Agency, Keplerlaan 1,
2201 AZ Noordwijk, The Netherlands

H. Dittus
Institute of Space Systems, German Aerospace Center
(DLR), Robert-Hooke-Strasse 7, 28359 Bremen, Germany

W. Ertmer · J. Hartwig · E. M. Rasel
Institute of Quantum Optics, Leibniz Universität Hannover,
Welfengarten 1, 30167 Hannover, Germany

M. Hauth · A. Peters · M. Schmidt · A. Senger
Humboldt-Universität zu Berlin, Unter den Linden 6,
10099 Berlin, Germany

S. Herrmann · T. Könemann · C. Lämmerzahl
Centre of Applied Space Technology and Microgravity
(ZARM), University of Bremen, Am Fallturm,
29359 Bremen, Germany

M. Inguscio · G. Modugno
European Laboratory For Non Linear
Spectroscopy (LENS), Via Nello Carrara,
1 50019 Sesto Fiorentino (FI), Italy

E. Kajari · W. P. Schleich
Institut für Quantenphysik, Universität Ulm,
Albert-Einstein-Allee 11, 89081 Ulm, Germany

A. Landragin · F. Pereira dos Santos
Observatoire de Paris,
SYRTE 61 avenue de l'Obseravtoire,
75014 Paris, France

M. Prevedelli
Dipartimento di Fisica dell'Università di Bologna,
Via Irnerio 46, 40126, Bologna, Italy

K. Sengstock
Universität Hamburg, Edmund-Siemers-Allee 1,
20146 Hamburg, Germany

R. Walser
Institut für Angewandte Physik,
Technische Universität Darmstadt,
Hochschulstr. 4a, 64289 Darmstadt, Germany

Published online: 23 September 2010

aspects of placing atom interferometers in space: the equipment needs, the realistically expected performance limits and potential scientific applications in a micro-gravity environment considering all aspects of quantum, relativistic and metrological sciences. A drop-tower compatible atom interferometry acceleration sensor prototype has been designed, and the manufacturing of its subsystems has been started. A compact modular laser system for cooling and trapping rubidium atoms has been assembled. A compact Raman laser module, featuring outstandingly low phase noise, has been realized. Possible schemes to implement coherent atomic sources in the atom interferometer have been experimentally demonstrated.

Keywords Atom interferometry · Inertial sensors

Introduction and Motivation

Matter-wave interferometry has recently led to the development of new techniques for the measurement of inertial forces, with important applications both in fundamental physics and applied research. The remarkable stability and accuracy that atom interferometers have reached for acceleration measurements can play a crucial role for science and technology. Quantum sensors based on atom interferometry had a rapid development during the last decade and different measurement schemes were demonstrated and implemented. Atom interferometry is used for precise measurements of the gravitational acceleration (Kasevich and Chu 1992; Peters et al. 1999; Müller et al. 2008), Earth's gravity gradient (Snadden et al. 1998; McGuirk et al. 2002), and rotations (Gustavson et al. 1997, 2000). Experiments on the validity of the equivalence principle (Fray et al. 2004) and on the measurement of the gravitational constant G (Bertoldi et al. 2006; Fixler et al. 2007; Lamporesi et al. 2007) have been performed, while tests of general relativity (Dimopoulos et al. 2007) and of Newton's $1/r^2$ law (Tino 2003; Ferrari et al. 2006) as well as the detection of gravitational waves (Tino and Vetrano 2007a; Dimopoulos et al. 2008, 2009) have been proposed. Accelerometers based on atom interferometry have been developed for many practical applications including metrology, geodesy, geophysics, engineering prospecting and inertial navigation (McGuirk et al. 2002; Peters et al. 2001; Bresson et al. 2006). Ongoing studies show that the space environment will allow us to take full advantage of the potential sensitivity of atom interferometers (Tino et al. 2007b; Turyshev et al. 2007).

Space Atom Interferometer (SAI) is a project of the European Space Agengy (ESA contract n. 20578/07/NL/VJ, AO-2004-064/082), with the main goal to demonstrate the possibility of applying such technology to future space missions.

Cold Atom Sensors

In analogy to optical interferometers, atomic matter-waves can be split and recombined giving rise to an interference signal. Different schemes have been used for splitting, reflecting and recombining atomic matter waves. In the SAI project, the Raman interferometer is chosen as the basic configuration (Kasevich and Chu 1992). This approach was proven to be the most successful so far in atom interferometry, at least for classical atom sources with respect to applications in precision experiments.

Figure 1 illustrates the basic principles of a matter-wave interferometry sensor based on laser cooled alkali atoms. Raman transitions change the internal hyperfine state and at the same time the external momentum state of the atom by two photon recoils. A sequence of three atom-light interaction processes can be applied to coherently split, redirect and recombine the atomic de Broglie wave. After the first beam splitter two atomic de Broglie waves emerge. Their relative momenta differ by the photon recoil transferred to the atom. By properly choosing the duration of the atom-light interaction, it is possible to equally split the incident waves ($\pi/2$ pulse) or entirely deflect the incident waves (π pulse). The atom interferometry sequence is indeed composed of a $\pi/2$ pulse acting as a beam splitter, a π pulse which redirects the atomic wavepackets, ant a final $\pi/2$ pulse recombining the matter waves propagating along the two arms of the interferometer. The two exit ports of the interferometer can be addressed and detected separately using spectroscopic techniques, e.g. by laser excitation and detection of the fluorescence emission.

The sensitivity of atomic sensors depends on the time interval T between pulses, during which the matter wave accumulates the phase along the interferometer trajectories (see Section "Baseline Structure of the SAI Sensor"). Laser cooling is therefore required to reach lower temperatures for a maximum extension of the interferometer time T as well as a high efficiency to achieve large numbers, N, of cold atoms. In absence of gravity the interferometer time is limited by the thermal expansion of the atoms through the experimental apparatus. For the lowest atomic temperatures (nK) presently reached, T can be as long as tens of seconds. On Earth, gravity is the major problem for cold atom

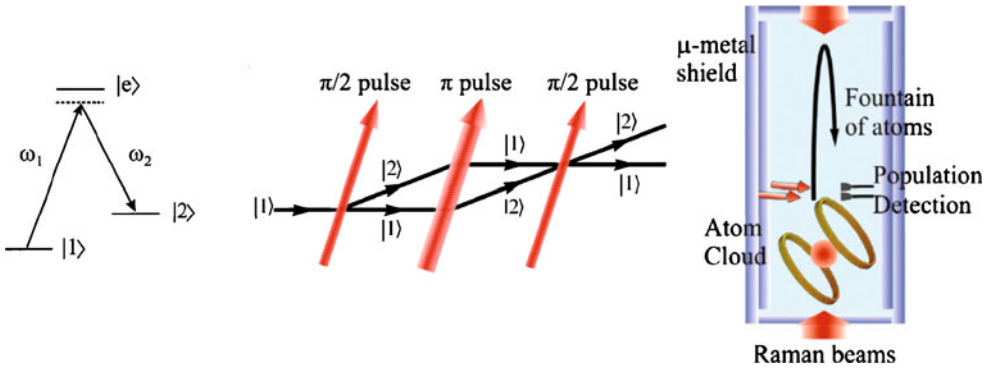

Fig. 1 Atom interferometry accelerometer; from *left to right*: Raman transition between the hyperfine levels of an alkali atom; Mach–Zender atom interferometry scheme implemented with three Raman pulses ($\pi/2 - \pi - \pi/2$): the direction of the *red arrows* represent the effective momentum transferred in the stimulated Raman process; typical scheme of an atom interferometry sensor operated under the Earth gravity: an atomic cloud is first trapped and cooled in an ultra-vacuum chamber; then it is launched in free flight and, after interacting with a Raman beams pair, it is finally probed by laser-induced fluorescence detection

optics: the free fall of about 5 m in one second restricts the measurement time well below 1 s.

The Transportable Atom Interferometer

The main goal of the SAI project is to demonstrate the technology readiness of atom interferometry inertial sensors for space applications. For this purpose, a compact prototype of single-axis accelerometer based on ultracold ^{87}Rb has been designed and is currently being assembled. At the same time, the project is investigating new schemes, based for example on quantum degenerate gases as source for the interferometer.

The realization of portable devices is the first step towards the development of space instruments based on matter wave interferometry. In addition, it will enable direct comparisons between atomic inertial sensors. Finally, SAI investigates emerging concepts such as pulsed and continuous atom lasers. With the most sensitive devices at hand, the project provides a unique framework to test the classical concepts of interferometry in combination with non-classical sources and to develop new strategies for employing quantum matter for precision measurements. Design target is to keep the prototype as compact as possible without degradation of sensitivity as compared to existing laboratory instruments. Besides portability, several properties of the sensor envisage future implementation in microgravity.

The prototype has been designed to be a vertical accelerometer, and allows both operation in microgravity and in ground tests. A sensitivity to accelerations of $\sim 10^{-7}$ m/s^2 at 1 s of integration time will be reached during ground testing of the instrument, with the interferometer time T limited to about 50 ms. Operating the same instrument in microgravity would allow a $\sim$100-fold improvement in the acceleration sensitivity, using an interaction time T of the order of 1 s.

Baseline Structure of the SAI Sensor

Space experiments impose strict limitations on the volume of the apparatus, on the weight, and on its power consumption. The final selection of materials, mechanical design, and implementation strategy takes into account all these requirements. The SAI sensor is a compact 1-axis accelerometer with sensitivity in the range of 10^{-8} g at 1 s. A modular laser system will be connected through optical fibers to a sensor head consisting of an ultra-high vacuum system with attached optics and of a magnetic shield. The same vacuum chamber is used for both trapping and cooling the atoms and to detect them at the end of the interferometric sequence. This scheme is mandatory to demonstrate possible future operation in microgravity, where the relative velocity between the atoms and the chamber will be null. On the other hand, the possibility of launching the atomic sample is important for ground testing of the instrument. The implementation of a 2D-MOT (Dieckmann et al. 1998) as source of cold atoms for a standard 3D-MOT ensures ultra-high vacuum conditions in the loading and interferometer regions, important for operating the sensor with coherent atomic sources such as a Bose-Einstein Condensate (BEC) and for testing its performance at long interrogation times.

The output phase of a Raman pulse matter-wave accelerometer is (Peters et al. 1999)

$$\phi = kaT^2 \tag{1}$$

where k is the wavevector associated to the Raman transitions (1.6×10^7 m^{-1} in Rb), a is the acceleration of the instrument platform and T is the time interval between Raman pulses. The phase resolution $\Delta\phi$ depends on the signal-to-noise ratio at detection; for high enough number of atoms, detection is limited by quantum projection noise and the phase resolution per shot is $\delta\phi \approx 1/\sqrt{N}$, giving a sensitivity to acceleration measurements of

$$\delta a = \frac{1}{\sqrt{N} k T^2}. \quad (2)$$

In ground tests, a typical measurement cycle with ~5 Hz repetition rate would consist in:

- launching ~10^8 atoms after loading for ~100 ms from the 2D-MOT;
- velocity and internal state selection resulting in ~10^6 atoms;
- interferometer sequence with duration $2T \sim$ 100 ms;
- detection of ~10^5 atoms with SNR ~100 (3 times worse than QPN);

resulting in virtual acceleration sensitivity of 10^{-7} m/s^2 at 1 s. In microgravity experiments, a typical measurement cycle would consist in:

- loading ~10^8 atoms in ~100 ms from the 2D-MOT;
- optical evaporative cooling to BEC for ~1 s resulting in ~10^6 atoms;
- interferometer sequence with duration $2T \sim 2$ s;
- detection of ~10^6 atoms with SNR ~300 (3 times worse than QPN);

resulting in virtual acceleration sensitivity of 10^{-10} m/s^2 per cycle.

In order to demonstrate technology readiness for space applications, the sensor is designed to fit into a standard capsule of the Bremen drop tower. The mechanical structure holding the vacuum system and all necessary optics shall be contained in a cylindrical volume with diameter ~60 cm and height ~150 cm.

Sensor Subsystems

The main subsystems of the SAI sensor are:

- mechanical structure of the sensor;
- vacuum system with a single chamber for atom trapping and interrogation/detection;
- high-flux source of cold atoms (2D-MOT);
- laser system for atom trapping and manipulation;
- Raman laser system for the atom interferometer operation;
- electronic control system.

Mechanical Structure and Main Vacuum System

Figure 2 shows a 3D drawing of the SAI sensor integrated in the drop-tower capsule. The main cell with a 20 cm tube for the interferometer sequence, the 2D-MOT system and the fiber collimators are well visible. A 1-1-1 configuration is chosen for the MOT, which allows to launch the atoms along the vertical. The short vertical tube above main chamber will allow to tune the interaction time and to operate the sensor as a

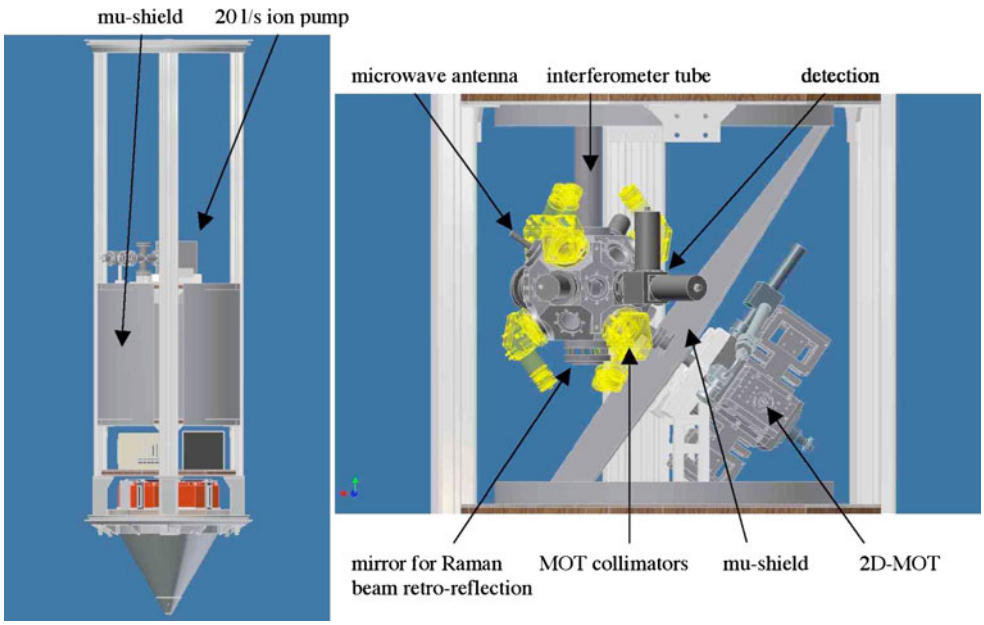

Fig. 2 3D views of the SAI sensor integrated into a drop-tower capsule

gradiometer for performance measurements. Since the interferometer sequence takes place close or within the main chamber, a μ-metal shield will enclose the whole vacuum system.

Main Vacuum System

The main vacuum chamber is shown in Fig. 3. It has 24 view-ports giving access for the cooling laser beams, the 2D-MOT atomic flux, the laser beams for optical BEC, the detection optics. In order to comply with geometrical constraints of the drop tower capsule, folded collimators are used to deliver the laser beams out of the optical fibres to the cell. The Raman beams propagate into the same polarization maintaining optical fibre, and will be delivered to the main chamber from a collimator placed at the end of the interferometer tube; the retro-reflecting mirror will be mounted below the main chamber. A precise tiltmeter will be rigidly attached to the mirror. Microwave excitation of atoms will be induced by an antenna placed outside a 30 mm diameter window in the horizontal symmetry plane of the main chamber. An ion pump for the main vacuum system will be mounted at the upper end of the 20 cm tube. Optical BK7 windows will be attached with indium wire sealing. This technology has already proved to be compatible with the acceleration loads of the Bremen drop tower (Vogel et al. 2006; van Zoest et al. 2010).

The vacuum system is contained in the central part of the drop-tower capsule, between two horizontal platforms that are connected by four vertical stringers. All kind of implemented components are rigidly mounted on the capsule platforms to withstand decelerations up to 50 g during the impact of the drop capsule at the end of the free fall. The main vacuum chamber is connected to the upper capsule platform through the vertical vacuum tube, that is made in titanium and has a thickness of 2.5 mm. The tube is clamped to the platform. Between the mechanical contact of the main chamber and the 2D-MOT vacuum cell an oscillation compensator (bellow) is inserted to additionally protect this ultra-high vacuum connection from longitudinal impact forces. The 2D-MOT system is connected to the lower capsule platform through an aluminum support attached to the massive square vacuum connector (see Fig. 6).

Magnetic Shield

Magnetic field gradients can introduce systematic shifts in the interferometer phase readout. Moreover, fluctuations in the magnetic field direction would influence the launching direction of atoms, degrading the sensor stability. Typical peak-to-peak magnetic field variations of 50 μT can be expected along the 100 m tube of the Bremen drop tower. These fields are strongly attenuated by the SAI μ-metal shield assembly. The shield consists of a set of two concentric boxes of high magnetic permeability material. An attenuation factor of 60 dB (both radially and axially) in the lower part of the tube, where the interferometer sequence will take place, is expected. The static field generated by the ion pump attached at the end of the 20 cm

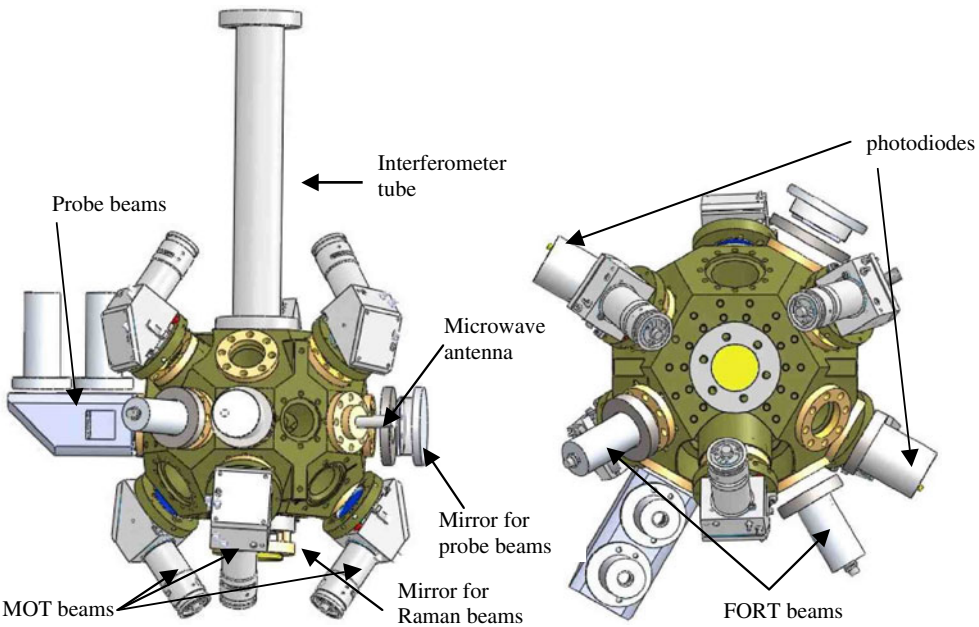

Fig. 3 3D views of the main vacuum chamber; FORT: far-off resonant optical dipole trap

titanium tube is attenuated by an additional 2 mm thick μ-metal shield. The main vacuum camber and the 2D-MOT assembly are separated by a double layer μ-metal wall, in order to get rid of the effect of metallic parts in the commercial Rb dispenser and to attenuate the static field generated by the small (2 l/s) ion pump attached to the 2D-MOT. The remaining metallic parts of 2D-MOT system are made of aluminum. Care has been taken to limit magnetic effects in the interferometer region, using the following considerations:

- strong permanent magnets (in ion pumps) are separately shielded;
- all mechanical components inside the main magnetic shield (main chamber, vacuum tubes, optical mounts) are made of non-magnetic materials;
- holes in main shield are small compared to their distance from the interferometer region.

As a consequence of the geometrical constraints given by the drop-tower capsule, the shape of the magnetic shield is not symmetric. Analytical formulas are not suited to precisely describe the magnetic field distribution within the shielded region. In order to find the optimal shape for the magnetic shield, we implemented a numerical model based on a commercial software (ANSYS). Goal of our analysis was to keep the residual field, in the region where the atom interferometry takes place, below 30 nT with an external applied field of 50 μT in either direction. As a result, the shape shown in Fig. 4 is well suited for our purposes. The shield consists of two nearly cylindrical μ-metal layers with 2 mm thickness, enclosing the whole vacuum system, and a double diagonal plane to separate the 2D-MOT from the main chamber. The distance between the two layers is 50 mm.

The mechanical structure, including the magnetic shield, shall be qualified for drop tower experiments. This gives additional constraints to the shape of magnetic shield. The assembly of μ-metal layers shall be able to withstand 50 g accelerations. Moreover, the shield cannot enclose the four vertical capsule stringers. The magnetic shield has been designed to fulfill such requirements, at the same time keeping the distance between μ-metal layers large enough to produce the desired shielding factor. The top and bottom covers of the cylindrical μ-metal layers are simply attached to the sides of the horizontal platforms, while the cylindrical layers and the diagonal walls are clamped to the platforms and to the stringers in several points. Typical results of our numerical calculations are illustrated in Fig. 5, which shows the computed field intensity distribution (expressed in T) for an external applied field of 50 μT in the vertical direction.

According to our calculations, the magnetic field is uniform in time and in space within 30 nT along the atom interferometry region during a free fall in the drop tower. The calculated shielding factor at the center of the main vacuum chamber has a minimum value of 6,000 along the vertical direction, due to the large aperture on the Raman beams path. The same analysis has been used to find a configuration of coils to produce a uniform bias field for the atom interferometry sequence.

The overall mass of the magnetic shield will be about 85 Kg.

High-Flux Atomic Source

The SAI 2D-MOT is derived from the designs implemented in the CASI experiment (http://www.iqo.uni-hannover.de/ertmer/casiindex/) and in the ATLAS experiment (http://www.iqo.uni-hannover.de/finaqs/index.php?n=WP1.IPulsedBosonicSource).

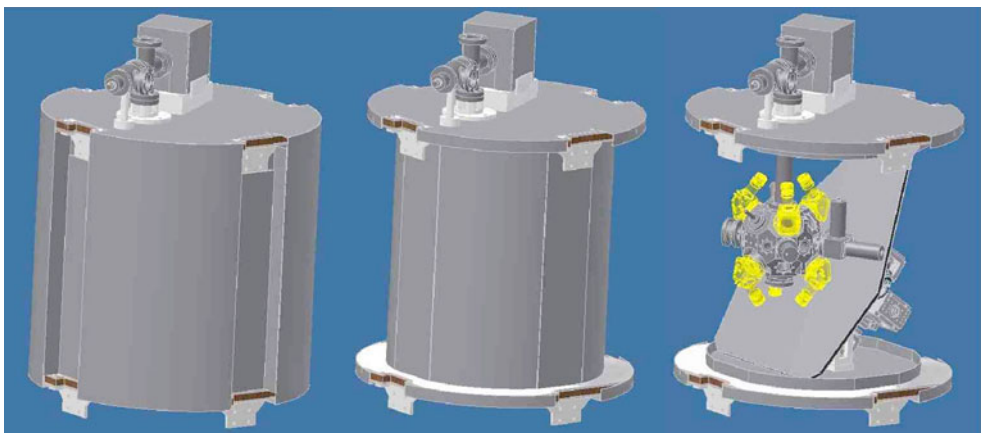

Fig. 4 3D views of the SAI magnetic shield; from *left to right*: fully assembled shield; with outer cylindrical layer removed; with inner cylindrical layer removed

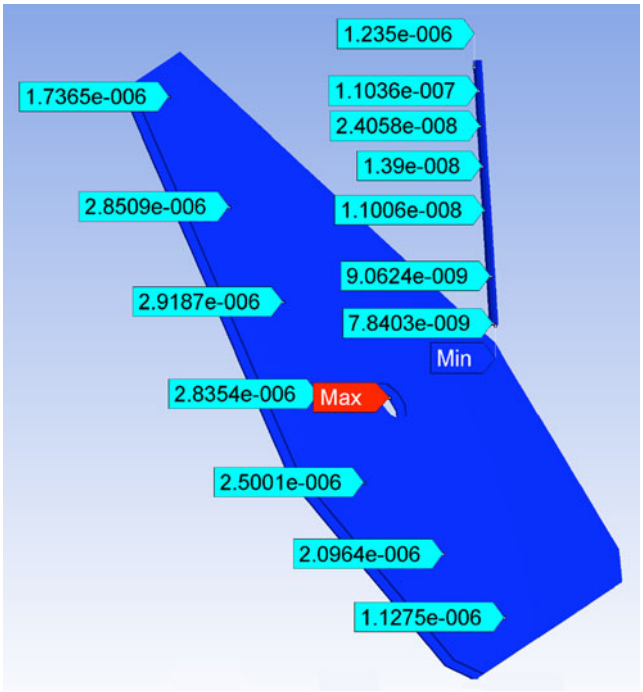

Fig. 5 Numerical calculation of residual magnetic field inside the capsule; the *labels* indicate the amplitude of magnetic field (in Tesla) on different points of the diagonal μ-metal plane and along the atomic trajectory (from the *center* of the chamber to the *upper edge* of the tube) when an external bias field of 50 μT is applied along the vertical axis

The SAI 2D-MOT system is based on a glass cell pressed on a non-magnetic aluminium body (see Fig. 6). The aluminium body will provide the interfaces for

- ion pump with a pumping speed of 2 l/s
- a turbomolecular pump, only used during the sensor assembly
- Rb reservoir
- bellow to the actual interferometer chamber.

The 2D-MOT of ATLAS and CASI are not equipped with a pump. CASI offers the possibility of initiation by a turbomolecular pump and uses a heatable Rb reservoir. ATLAS uses dispensers rather than Rb reservoirs. Both CASI and ATLAS use a rigid connector to the main chamber. Differently from the above mentioned experiments, the SAI 2D-MOT will be connected to the main chamber via a bellow and it will have an additional 2 l/s ion pump. The 2D-MOT structure also serves as mount for the four telescopes, shaping the laser beams for cooling the atoms in the transverse direction to the atomic beam, and for the 2D-MOT coils.

Laser System

The laser system for cooling and detecting Rb atoms is split into five compact modules as shown in Fig. 7. The Raman laser beams for the interferometer sequence are generated in an additional module, described in Section "Raman Laser System".

In the master module, a laser is stabilised on the Rb FM spectroscopy signal and sent to a second module, where it is amplified. This light is used as a reference for an offset-lock in the repumper module and in the Raman laser system; in addition, it is also forwarded to the 2D-MOT and 3D-MOT laser modules. The two MOT modules shift the master frequency to the cooling frequency and amplify it, in addition allowing a control of the laser detuning from resonance and of laser power. Finally, they distribute the cooling and

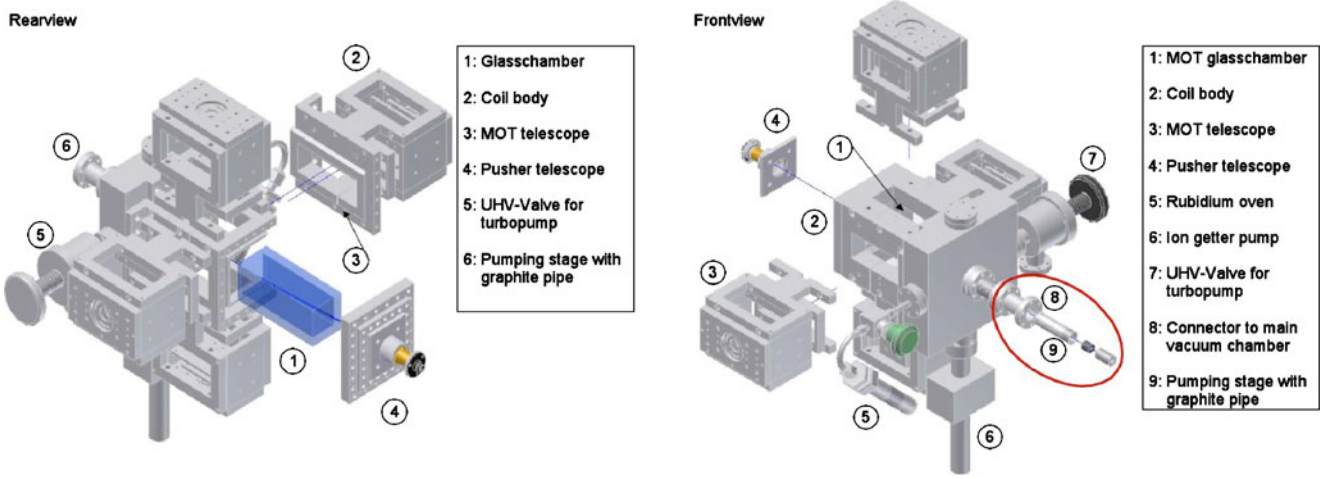

Fig. 6 3D views of the mechanical structure of the 2D-MOT system

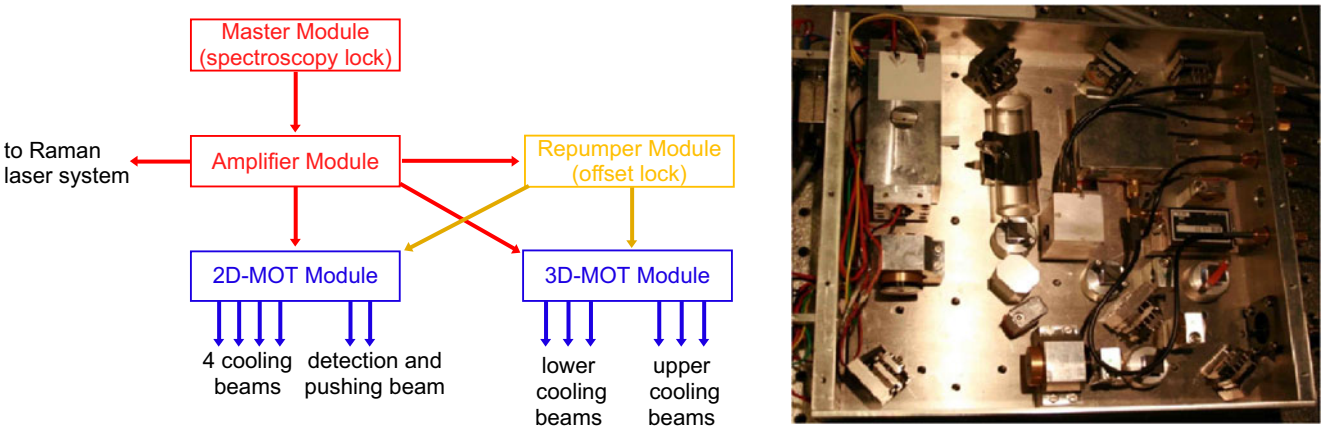

Fig. 7 *Left*: scheme of the modular laser system; *right*: a picture of the master laser module

repumping light onto several outputs. The arrows in Fig. 7 represent optical fibre connections.

The dimensions of all modules are listed in Table 1. Each module was designed and optimised for compactness and robustness. The beam height was set to only 2 cm and mounts and frames created of robust aluminium. The mounts had already been developed and tested under drop-tower conditions in the framework of the QUANTUS project (Vogel et al. 2006; van Zoest et al. 2010). Figure 7 also shows the master module fully assembled.

Extended Cavity Lasers (ECLs) are used in the SAI laser system. These lasers, based on an interferential filter for wavelength selection (Baillard et al. 2006), offer the narrow linewidth of conventional grating-based ECLs, but they are more than one order of magnitude less sensitive to misalignment. This characteristic makes them ideal for implementation in mobile laser systems, where mechanical stability is of paramount importance.

Raman Laser System

In order to induce a two-photon optical Raman transition on the hyperfine ground state of rubidium, a pair of two lasers with a fixed phase relation, a frequency difference of approximately 6.8 GHz and a wavelength of 780 nm is required. The most obvious method to achieve this is to phase lock two lasers onto each other. An optical phase-locked loop (OPLL) has become the standard for atom interferometry experiments in various laboratories and is also the baseline setup for SAI.

Table 1 Laser module dimensions

Module	Width [mm]	Depth [mm]	Height [mm]
Master module	236	250	63
Amplifier module	240	190	66
Repumper module	186	260	63
2D-MOT module	350	260	73
3D-MOT module	350	260	73
Raman module	430	430	106

Optomechanical Implementation and OPLL

The Raman laser optical setup contains two ECLs. The Raman master laser is overlapped on a photodiode with the reference laser generated by the module described in Section "Laser System". The resulting beat note signal is locked on a frequency reference provided by the frequency synthesis chain described in Section "Reference Frequency Chain". The second ECL (slave) is overlapped with the master laser and their beat note is phase locked to the low phase noise signal at 6.8 GHz (hyperfine splitting of ^{87}Rb) provided by a frequency synthesis chain (see Section "Reference Frequency Chain"). Since the phase difference between Raman master and slave lasers is imprinted directly on the atoms, phase noise performance of both the frequency reference and the optical phase locked loop are of key importance for the sensor performance. It is therefore imperative to minimize the residual phase noise between the two lasers. The specified acceleration sensitivity of SAI (10^{-7} m/s^2 in 1 s) corresponds to a maximum allowed phase noise spectral density of -95 dBrad^2/Hz between 10 Hz and 10 kHz.

The phase noise has been measured from an out-of-loop comparison between the Raman beat note and the reference 6.8 GHz source. As shown in Fig. 8, the phase noise spectral density for the OPLL stays below a level of -120 dBrad^2/Hz (1 µrad/$\sqrt{\text{Hz}}$) between 100 Hz and 60 kHz, well compatible with the noise level required by SAI. To our knowledge, the measured OPLL phase

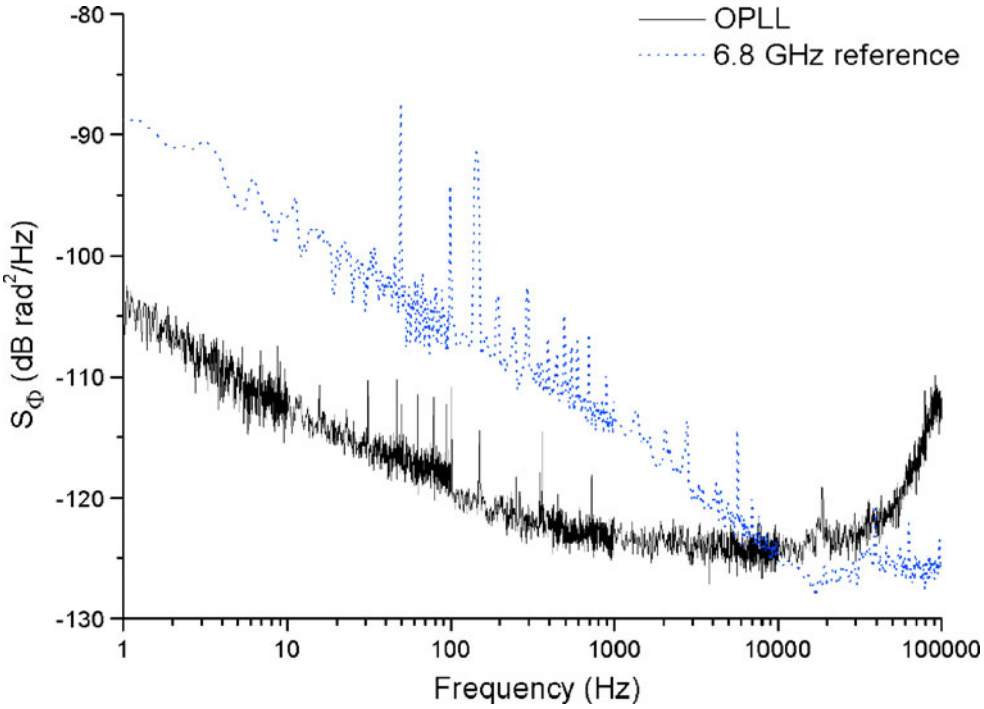

Fig. 8 Phase noise spectral density of the Raman laser OPLL (*solid line*) and of the 6.8 GHz frequency chain (*dashed line*)

noise is among the lowest levels ever reached (Cheinet et al. 2008). The achieved locking bandwidth is slightly above 4 MHz. If this OPLL phase noise was the main contributing factor to overall accelerometer sensitivity, a single-shot sensitivity $\delta a/a$ of 2×10^{-10} would be achieved.

Both the master and the slave laser beams are finally amplified in two separate tapered amplifiers (TA).

Reference Frequency Chain

A microwave frequency source is used to generate the reference for the optical phase-locked loop (OPLL) of the Raman lasers. With typical bandwidths of the OPLL of several MHz, the phase stability of the microwave source reduces drastically the relative phase fluctuations of the lasers. Still, small phase fluctuations of this reference source will limit the sensitivity of the interferometer, in a way that depends on the interferometer parameters (interferometer duration, duration of the Raman pulses, etc.). As the repetition rate of an atom interferometer experiment lies between a fraction of a Hz and few Hz, requirements on the phase noise at low frequency are stringent, and state of the art oscillators are necessary. A conventional solution consists in generating a microwave reference by multiplication of ultra-low noise quartz oscillators. This signal can then be compared directly to the optical beat note, or can be used to phase lock a microwave oscillator such as an Yttrium Indium Garnet (YIG) or a Dielectric Resonator Oscillator (DRO) onto the quartz signal. This last solution offers the possibility to realize a tunable frequency source, whose phase and/or frequency can be easily modulated. Also, it improves the phase noise at high frequencies. Better performances can be obtained using sapphire oscillators.

The contribution of the microwave source onto the phase noise of the interferometer can be reduced down to about 1 mrad/shot for $2T = 100$ ms, using commercial ultra low noise quartz oscillators of various classes (BlueTop from Wenzel, or BVA from Oscilloquartz). When extrapolating the performances of an atom interferometer to larger interrogation times ($2T \leq 1$ s), the phase noise at low frequency will be the dominant contribution. The BVA quartz appears here as the best solution among the different types of commercial low phase noise quartz oscillators. Assuming a phase noise scaling as $1/f^2$ for frequencies below 10 Hz, the expected sensitivity per shot of the interferometer scales linearly with T. We calculate from the specifications of the OCXO 8607 from Oscilloquartz an interferometer phase noise of 9 mrad/shot for $T = 1$ s. As for the microwave frequency synthesis, its contribution can be reduced to less than 1 mrad/shot by a careful design, independent of T.

The source consists in a reference signal at 100 MHz, obtained by phase locking a 100 MHz quartz onto a 5 MHz BVA oscillator. This double quartz system is necessary to obtain the lowest level of phase noise both in the low and high frequency range.

The 100 MHz signal is then be multiplied by 2, amplified and sent to a Non Linear Transmission Line (NLTN), which generates a comb of frequencies, harmonics of 200 MHz. The 6.8 GHz tooth of the comb is then filtered, amplified, and used to phase lock a DRO with an offset frequency provided by a Direct Digital Synthesizer (DDS1). The DRO is thus phase and frequency tunable. A second DDS is used as the reference of the OPLL.

The multiplication stage is therefore composed of two stages:

- a Radio Frequency (RF) stage with a $\times 2$ multiplier (RK3+ from MiniCircuits), a band pass filter at 200 MHz (BL Microwave B0200-100C1BS), an RF amplifier (ERA 5 from MiniCircuits), a low pass passive filter at 250 MHz (MiniCircuits);
- a microwave (MW) stage with a comb generator (NLTL from Picosecond Pulse Labs), a band pass filter at 6.8 GHz (BL Microwave BP6800-70-6-CS or 7 GHz BP7000-70-6-CS), a MW amplifier (AML612L3401 from AML Communications).

The band pass filter in the MW stage is narrow enough to select only one line of the frequency comb (the bandwidth of the filter is 70 MHz).

For a frequency offset from the carrier lower than 10 kHz, the RF stage limits the global phase noise of the multiplication stage. For a larger frequency the noise introduced by the MW stage appears. The resulting phase noise is shown in Fig. 8.

Electronic Control System

We have developed a versatile source of signals able to control the different phases of a cold atom experiment. It is based upon a series of parallel modules, generating parallel signals referred to the same clock. The output of each module is generated by a Field Programmable Gate Array (FPGA). This device can be integrated in a stand-alone 19" rack. It can accept up to 8 Signals Generator Modules (SGM), and uses an Interface Control Module (ICM) to load programming data and controls from the serial port interface of a PC. Depending on its type, each module can supply up to 16 output channels. Each channel can output a sequential 32-step signal. Each step can be programmed from 1 μs to 10 s duration without any restriction on the other channels. The overall control system of the SAI sensor will consist of three analog modules (12 analog output channels), three TTL modules (24 TTL output channels) and 8 single-channel DDS boards.

Coherent Atomic Source

The SAI sensor design also provides the possibility of integrating a coherent atomic source. Using a BEC will enable a much longer interaction time when operating the atom interferometer in microgravity. All-optical BEC has been implemented in a separate experiment using a fiber laser at 1,565 nm (Clément et al. 2009). The additional subsystems for the optical BEC consist of a commercial 1,565 nm high-power CW fiber laser and of two telescopes, attached to the main chamber, to produce a pair of crossing focused beams in the position of the MOT.

All-optical techniques allow fast productions of BEC compared with magnetic traps, and optical potentials can trap atoms whatever their spin. The chosen method is finally quite simple; neither additional cooling (such as Raman sideband cooling), nor magnetic fields are required, nor movable optical parts to compress the optical trap. Only molasses and compressed-MOT phases are needed to get a good loading before performing an evaporation stage until the phase transition. The keypoint of such setup is the specific light-shift features at this wavelength for ^{87}Rb. Transitions from $^5P_{3/2}$ to $4D$ states at 1,529 nm induce strong light-shift for the $^5P_{3/2}$ levels. Light-shift of the upper level of the cooling transition $^5P_{3/2}$ is nearly 42 times stronger than the light-shift of the ground state. The effect of 1,565 nm light on the cooling transition allows a loading procedure with simultaneous cooling and trapping.

Conclusions

We have designed a compact and transportable prototype of atom interferometry accelerometer, to demonstrate the possibility to apply such technology in future space missions. The system in under construction, and several subsystems have already been completed and tested. The Space Atom Interferometer project will provide a valuable insight into the potential of atom interferometry for space applications.

Acknowledgements This work was supported by ESA through the SAI project (contract no. 20578/07/NL/VJ).

References

Baillard, X., Gauguet, A., Bize, S., Lemonde, P., Laurent, P., Clairon, A., Rosenbusch, P.: Interference-filter-stabilized external-cavity diode lasers. Opt. Coom. **266**, 609–613 (2006)

Bertoldi, A., Lamporesi, G., Cacciapuoti, L., De Angelis, M., Fattori, M., Petelski, T., Peters, A., Prevedelli, M., Stuhler, J., Tino, G.M.: Atom interferometry gravity-gradiometer for

the determination of the Newtonian gravitational constant G. Eur. Phys. J. D. **40**, 271 (2006)
Bresson, A., Bidel, Y., Bouyer, P., Leone, B., Murphy, E., Silvestrin, P.: Quantum mechanics for space applications. Appl. Phys. B **84**, 545–550 (2006)
Cheinet, P., Canuel, B., Santos, F.P.D., Gauguet, A., Leduc, F., Landragin, A.: Measurement of the sensitivity function in time-domain atomic interferometer. IEEE Trans. Instrum. Meas. **57**, 1141 (2008)
Clément, J.F., Brantut, J.P., Robert de Saint Vincent, M., Varoquaux, G., Nyman, R.A., Aspect, A., Bourdel, T., Bouyer, P.: All-optical runaway evaporation to Bose-Einstein condensation. Phys. Rev. A **79**, 61406 (2009)
Dieckmann, K., Spreeuw, R.J.C., Weidemüller, M., Walraven, J.T.M.: Two-dimensional magneto-optical trap as a source of slow atoms. Phys. Rev. A **58**, 3891 (1998)
Dimopoulos, S., Graham, P., Hogan, J., Kasevich, M.: Testing general relativity with atom interferometer. Phys. Rev. Lett. **98**, 111102 (2007)
Dimopoulos, S., Graham, P.W., Hogan, J.M., Kasevich, M.A., Rajendran, S.: Atomic gravitational wave interferometric sensor. Phys. Rev. D **78**, 122002 (2008)
Dimopoulos, S., Graham, P.W., Hogan, J.M., Kasevich, M.A., Rajendran, S.: Gravitational wave detection with atom interferometry. Phys. Lett. B **678**, 37–40 (2009)
Ferrari, G., Poli, N., Sorrentino, F., Tino, G.M.: Long-lived Bloch oscillations with Bosonic Sr atoms and application to gravity measurement at the micrometer scale. Phys. Rev. Lett. **97**, 060402 (2006)
Fixler, J.B., Foster, G.T., McGuirk, J.M., Kasevich, M.: Atom interferometer measurement of the Newtonian constant of gravity. Science **315**, 74 (2007)
Fray, S., Alvarez Diez, C., Hänsch, T.W., Weitz, M.: Atomic interferometer with amplitude gratings of light and its applications to atom based tests of the equivalence principles. Phys. Rev. Lett. **93**, 240404 (2004)
Gustavson, T.L., Bouyer, P., Kasevich, M.: Precision rotation measurements with an atom interferometer gyroscope. Phys. Rev. Lett. **78**, 2046 (1997)
Gustavson, T.L., Landragin, A., Kasevich, M.: Rotation sensing with a dual atom-interferometer Sagnac gyroscope. Class. Quantum Gravity **17**, 2385 (2000)
Kasevich, M., Chu, S.: Measurement of the gravitational acceleration of an atom with a light-pulse atom interferometer. Appl. Phys. B **54**, 321 (1992)
Lamporesi, G., Bertoldi, A., Cacciapuoti, L., Prevedelli, M., Tino, G.M.: Determination of the Newtonian gravitational constant using atom interferometry. Phys. Rev. Lett. **100**, 050801 (2007)
McGuirk, J.M., Foster, G.T., Fixler, J.B., Snadden, M.J., Kasevich, M.A.: Sensitive absolute-gravity gradiometry using atom interferometry. Phys. Rev. A **65**, 033608 (2002)
Müller, H., Chiow, S.W., Herrmann, S., Chu, S., Chung, K.-Y.: Atom interferometry tests of the isotropy of post-Newtonian gravity. Phys. Rev. Lett. **100**, 031101 (2008)
Peters, A., Chung, K.Y., Chu, S.: Measurement of gravitational acceleration by dropping atoms. Nature **400**, 849 (1999)
Peters, A., Chung, K.Y., Chu, S.: High-precision gravity measurements using atom interferometry. Metrologia **38**, 25 (2001)
Snadden, M.J., McGuirk, J.M., Bouyer, P., Haritos, K.G., Kasevich, M.A.: Measurement of Earth's gravity gradient with an atom interferometer-based gravity gradiometer. Phys. Rev. Lett. **81**, 971 (1998)
Tino, G.M.: 2001: a relativistic spacetime odyssey. In: Ciufolini, I., Dominici, D., Lusanna, L. (eds.) High Precision Gravity Measurements by Atom Interferometry—Proceedings of JH Workshop, Firenze 2001. World Scientific (2003)
Tino, G.M., Vetrano, F.: Is it possible to detect gravitational waves with atom interferometers? Class. Quantum Gravity **24**, 2167–2177 (2007a)
Tino, G.M., et al.: Atom interferometers and optical atomic clocks: new quantum sensors for fundamental physics experiments in space. Nucl. Phys. B Proc. Suppl. **166**, 159–165 (2007b)
Turyshev, S.G., Israelsson, U.E., Shao, M., Yu, N., Kusenko, A., Wright, E.L., Everitt, C.W.F., Kasevich, M.A., Lipa, J.A., Mester, J.C., Reasenberg, R.D., Walsworth, R.L., Ashby, N., Gould, H., Paik, H.-J.: Space-based research in fundamental physics and quantum technologies. Int. J. Mod. Phys. D **16**, 1879 (2007)
van Zoest, T., Gaaloul, N., Singh, Y., Ahlers, H., Herr, W., Seidel, S.T., Ertmer, W., Rasel, E., Eckart, M., Kajari, E., Arnold, S., Nandi, G., Schleich, W.P., Walser, R., Vogel, A., Sengstock, K., Bongs, K., Lewoczko-Adamczyk, W., Schiemangk, M., Schuldt, T., Peters, A., Könemann, T., Müntinga, H., Lämmerzahl,C., Dittus, H., Steinmetz, T., Hänsch, T.W., Reichel, J.: Bose–Einstein Condensation in Microgravity Science, vol. 328, p. 1540 (2010)
Vogel, A., Schmidt, M., Sengstock, K., Bongs, K., Lewoczko, W., Schuldt, T., Peters, A., Van Zoest, T., Ertmer, W., Rasel, E., Steinmetz, T., Reichel, J., Könemann, T., Brinkmann, W., Göklü, E., Lämmerzahl, C., Dittus, H.J., Nandi, G., Schleich, W.P., Walser, R.: Bose-Einstein condensates in microgravity. Appl. Phys. B **84**(4), 663–671 (2006)